平成 29 年度　学位論文

論文題目

Atorvastatin reduces cardiac and adipose tissue inflammation in rats with metabolic syndrome

(アトルバスタチンはメタボリックシンドロームラットにおいて、心臓や脂肪組織炎症を減少させる)

名古屋大学大学院医学系研究科

医療技術学専攻

(指導：永田　浩三　教授)

山田　雄一郎

要旨

背景—スタチンはコレステロール生合成を強力に抑制し、心血管疾患の発症を抑制する。スタチンはまた、コレステロール低下作用とは独立して、抗炎症作用を含む多面的な効果を発揮することが知られている。しかし、これらの多面的効果の基礎にある分子メカニズムはいまだ明らかではない。

方法および結果—Dahl 食塩感受性ラットと Zucker ラットの交配に由来するメタボリックシンドローム（MetS）の動物モデルである DahlS.Z-*Lepr*^{fa}/*Lepr*^{fa} (DS/obese)ラットに生後 9 週齢より vehicle、スタチンの一種であるアトルバスタチンを低用量（6 mg/kg）または高用量（20 mg/kg）で連日強制経口投与し、生後 13 週齢において種々の解析を行った。ヘテロ個体(DahlS.Z-*Lepr*^{fa}/*Lepr*$^{+}$)同士の交配で生まれる DahlS.Z-*Lepr*$^{+}$/*Lepr*$^{+}$(DS/lean)にも vehicle を投与し、対照動物として比較検討した。低用量および高用量のアトルバスタチンは、心筋線維化、左室拡張障害、心筋酸化ストレスと炎症、および脂肪組織炎症を改善した。高用量のアトルバスタチンは低用量よりも強力に脂肪細胞肥大を減少させた。アトルバスタチンは脂肪組織におけるペルオキシソーム増殖因子活性化受容体ガンマ（PPARγ）の遺伝子発現を抑制し、血清アディポネクチン濃度を減少させた。また、アトルバスタチンは DS/obese ラットの心臓において AMP 活性化プロテインキナーゼ（AMPK）を活性化するとともに、転写因子である核内因子カッパ B（NF-κB）を不活性化した。DS/obese ラットの脂肪組織においてアトルバスタチンの投与により、AMPK 活性の低下は抑制され、NF-κB 活性の低下はさらに増強した。

結論—本 MetS ラットモデルにおいてアトルバスタチンの心臓および脂肪組織に対する抗炎症効果の少なくとも一部は、AMPK 活性の増加と NF-κB 活性の低下に起因することが示唆された。

Abstract

Background: Statins are strong inhibitors of cholesterol biosynthesis and help to prevent cardiovascular disease. They also exert additional pleiotropic effects that include an anti-inflammatory action and are independent of cholesterol, but the molecular mechanisms underlying these additional effects have remained unclear. We have now examined the effects of atorvastatin on cardiac and adipose tissue inflammation in DahlS.Z-*Lepr*^{fa}/*Lepr*^{fa} (DS/obese) rats, which we previously established as a model of metabolic syndrome (MetS).

Methods and Results: DS/obese rats were treated with atorvastatin (6 or 20 mg kg^{-1} day^{-1}) from 9 to 13 weeks of age. Atorvastatin ameliorated cardiac fibrosis, diastolic dysfunction, oxidative stress, and inflammation as well as adipose tissue inflammation in these animals at both doses. The high dose of atorvastatin reduced adipocyte hypertrophy to a greater extent than did the low dose. Atorvastatin inhibited the up-regulation of peroxisome proliferator–activated receptor γ gene expression in adipose tissue as well as decreased the serum adiponectin concentration in DS/obese rats. It also activated AMP-activated protein kinase (AMPK) as well as inactivated nuclear factor–κB (NF-κB) in the heart of these animals. The down-regulation of AMPK and NF-κB activities in adipose tissue of DS/obese rats was attenuated and further enhanced, respectively, by atorvastatin treatment.

Conclusions: The present results suggest that the anti-inflammatory effects of atorvastatin on the heart and adipose tissue are attributable at least partly to increased AMPK activity and decreased NF-κB activity in this rat model of MetS.

1. Introduction

Metabolic syndrome (MetS) is a cluster of conditions that are associated with cardiovascular morbidity and mortality. Chronic inflammation is a common feature of MetS, with inflammatory signals emanating from visceral adipose tissue as the fat deposit expands as a result of chronic positive energy balance. Both adipocytes and macrophages within adipose tissue secrete numerous hormones and cytokines that contribute to the pathophysiology of MetS, and local inflammation within fat may trigger systemic inflammation and insulin resistance. The event that triggers such adipose tissue inflammation remains unclear, although fat-derived cytokines, such as leptin and interleukin-6, may participate directly in endothelial cell activation and inflammation in the cardiovascular system.

Statins inhibit 3-hydroxy-3-methylglutaryl coenzyme A (HMG-CoA) reductase and thereby block cholesterol biosynthesis and help to prevent atherosclerotic cardiovascular disease, with their clinical benefit having been demonstrated in clinical trials such as the Heart Protection Study (HPS) [1] and West of Scotland Coronary Prevention Study (WOSCOPS) [2]. In addition to their cholesterol-lowering action, statins have been proposed to exert anti-oxidative and cardioprotective effects [3, 4]. They also have anti-inflammatory effects [5] as well as activate AMP-activated protein kinase (AMPK) in vitro and in vivo [6]. Simvastatin exerts an anti-inflammatory effect through activation of the protein kinase Akt and subsequent generation of nitric oxide by endothelial nitric oxide synthase [7]. AMPK signaling inhibits inflammatory responses elicited by the nuclear factor–κB (NF-κB) system [8]. However, the molecular mechanisms underlying the anti-inflammatory actions of statins have remained largely unclear. Moreover, the effects of statins on glucose metabolism

including insulin resistance have been unresolved [9]. Treatment with atorvastatin (25 or 50 mg kg^{-1} day^{-1}) for 3 weeks enhanced insulin sensitivity in a dose-dependent manner in Zucker fatty and lean rats [10]. Treatment with pravastatin (100 mg kg^{-1} day^{-1}) over 24 weeks had a moderate lipid-lowering effect as well as prevented the onset of diabetes mellitus and left ventricular (LV) diastolic dysfunction in association with amelioration of cardiac oxidative stress and normalization of adipokine profiles in a rat model of insulin resistance. In contrast, atorvastatin (100 mg kg^{-1} day^{-1}) had a pronounced lipid-lowering effect but did not retard the progression of insulin resistance or LV diastolic dysfunction in this model [11]. These findings thus suggest that the pleiotropic effects of statins might be dependent on the dose or duration of treatment in animal models of insulin resistance [12], with the mechanisms underlying such effects remaining unknown.

We have established the DahlS.Z-*Lepr*^{fa}/*Lepr*^{fa} (DS/obese) rat, derived from a cross between Dahl salt-sensitive and Zucker rats, as an animal model of MetS [13]. In addition to a MetS-like condition, which is characterized by adipocyte hypertrophy and adipose tissue inflammation, these rats develop salt-sensitive hypertension and LV diastolic dysfunction as well as LV hypertrophy and fibrosis, with these alterations being associated with increased cardiac oxidative stress and inflammation [14-17]. The aim of the present study was to examine and characterize the effects of atorvastatin at two different doses on cardiac and adipose tissue pathology and metabolism in DS/obese rats.

2. Methods

2.1. Animals

Male inbred DS/obese rats at the age of 9 weeks were randomly assigned to three groups: those treated with vehicle (MetS group) or with a low (6 mg/kg, ATV-L group) or high (20 mg/kg, ATV-H group) dose of atorvastatin. Age-matched male homozygous lean littermates of DS/obese rats (DahlS.Z-*Lepr*$^{+}$/*Lepr*$^{+}$, or DS/lean, rats) treated with vehicle served as control animals (CONT group). Atorvastatin (Pfizer, Peapack, NJ) or vehicle (0.5% methyl cellulose solution) was administered daily by oral gavage from 9 to 13 weeks of age. At 13 weeks, an oral glucose tolerance test (OGTT) and an insulin tolerance test (ITT) were conducted and organ harvesting was performed for analysis as described previously [17].

2.2. Echocardiography and Hemodynamics

Systolic blood pressure (SBP) was monitored once a week in conscious animals by the tail-cuff plethysmography (BP-98A; Softron, Tokyo, Japan). At the age of 13 weeks, rats were subjected to transthoracic echocardiography [18] and subsequent cardiac catheterization [19]. A more detailed description of methodology is provided elsewhere [15].

2.3. Histology and Immunohistochemistry

LV and visceral (retroperitoneal) fat tissue were processed for histological analysis as described previously [16]. Immunohistochemical staining for the monocyte-macrophage marker CD68 in LV and adipose tissue sections was also performed and all images were analyzed as described previously [16].

2.4. Biochemistry

Blood specimen were collected and metabolic parameters were measured as described [20]. The homeostasis model assessment of insulin resistance (HOMA-IR) and of β-cell function (HOMA-β) were calculated as described previously [21].

2.5. Assay of Superoxide Production

Superoxide production in LV tissue sections was measured by dihydroethidium (Sigma, St. Louis, MO) staining as described [22]. A more detailed description of principle and methodology is provided elsewhere [23].

2.6. Quantitative RT-PCR

Quantitative reverse transcription (RT) and polymerase chain reaction (PCR) analysis of LV and visceral fat tissue was performed as described previously [16] with specific primers for cDNAs encoding atrial natriuretic peptide (ANP) [18], brain natriuretic peptide (BNP) [18], collagen type I and type III [24], connective tissue growth factor (CTGF) [25], transforming growth factor–β1 (TGF-β1) [18], the $p22^{phox}$ [26], $gp91^{phox}$ [26], and Rac1 [14] subunits of NADPH oxidase, monocyte chemoattractant protein–1 (MCP-1) [25], cyclooxygenase-2 (COX-2) [26], adiponectin, peroxisome proliferator–activated receptor γ (PPARγ), and sterol regulatory element–binding protein–1c (SREBP-1c) (Supplemental Table S1). Reagents for detection of human 18S rRNA (Applied Biosystems, Foster City, CA) were used to quantify rat 18S rRNA as an internal standard.

2.7. Immunoblot Analysis

Total protein was isolated from LV and visceral fat tissue and quantitated with the use of the Bradford reagent (Bio-rad, Hercules, CA). A more detailed description of methodology is provided elsewhere [20]. The membrane was incubated with a 1:200 dilution of mouse monoclonal antibodies to PPARγ (Santa Cruz Biotechnology, Dallas, TX) or with 1:1000 dilutions of rabbit monoclonal antibodies to glyceraldehyde-3-phosphate dehydrogenase (GAPDH) (Cell Signaling Technology, Beverly, MA). The other antibodies were described previously [20, 27].

2.8. Statistics

Data are expressed as means ± SEM. Differences among groups of rats at the age of 13 weeks-were assessed with one-way factorial analysis of variance (ANOVA) and Fisher's multiple-comparison test. The time courses of sequential data were compared among groups by two-way repeated-measures ANOVA. A *P* value less than 0.05 was considered statistically significant.

3. Results

3.1. Physiology and Cardiac Morphology and Function

Body weight, food intake, and SBP were increased in DS/obese rats compared with DS/lean rats at 9 weeks of age and thereafter and were not affected by atorvastatin (Figure 1A–C). At 13 weeks, there were no significant differences in the ratios of heart or LV weight to tibial length (indices of cardiac and LV hypertrophy, respectively) as well as those of visceral (retroperitoneal, epididymal, and mesenteric) or subcutaneous (inguinal) fat weight to tibial length among the MetS, ATV-L, and ATV-H groups (Supplemental Table S2).

Echocardiography revealed that the thickness of the interventricular septum and LV posterior wall, LV mass, relative wall thickness, LV fractional shortening, and LV ejection fraction were all similar in the MetS, ATV-L, and ATV-H groups (Supplemental Table S3). The deceleration time, isovolumic relaxation time and tau were shortened and both LV end-diastolic pressure (LVEDP) and the ratio of LVEDP to LV end-diastolic dimension, an index of LV diastolic stiffness, were reduced in the ATV-L and ATV-H groups in comparison with the MetS group (Supplemental Table S3).

3.2. Lipid and Glucose Metabolism

Both low and high doses of atorvastatin lowered the serum concentrations of total cholesterol, LDL-cholesterol, triglyceride, and free fatty acids (FFAs), but not that of HDL-cholesterol (Table 1). No significant difference in the fasting serum concentration of glucose was detected among the three experimental groups (Table 1). The fasting insulin concentration in serum and HOMA-IR and HOMA-β indices were all reduced in the ATV-L and ATV-H groups in comparison with the MetS group (Table 1). OGTT and ITT curves showed that both the glucose intolerance and insulin resistance apparent in MetS rats were ameliorated by atorvastatin treatment (Figure 1D, E).

3.3. Cardiomyocyte Hypertrophy and Cardiac Fibrosis

Microscopic examination showed that the cross-sectional area of LV cardiomyocytes in MetS rats was unchanged by atorvastatin treatment at either dose (Supplemental Figure S1A, B). However, the abundance of ANP and BNP mRNAs in the heart was down-regulated by atorvastatin at both doses (Supplemental Figure S1C, D). Azan-Mallory staining showed that fibrosis in perivascular and interstitial regions of the LV myocardium was reduced in the ATV-L and ATV-H groups compared with the MetS group (Supplemental Figure S1E–H). The abundance of collagen types I and III, CTGF, and TGF-β1 mRNAs in LV tissue was also decreased in the ATV-L and ATV-H groups in comparison with the MetS group (Supplemental Figure S1I–L).

3.4. Cardiac Oxidative Stress and Inflammation

Both doses of atorvastatin reduced the extent of both superoxide production in myocardial tissue sections and the activity of NADPH oxidase in LV homogenates of MetS rats (Supplemental Figure S2A–C). The amounts of mRNAs for the $p22^{phox}$ and $gp91^{phox}$ membrane components and for the Rac1 cytosolic component of NADPH oxidase in the left ventricle were also down-regulated in the ATV-L and ATV-H groups

in comparison with the MetS group (Supplemental Figure S2D–F).

Immunohistochemical staining for CD68 showed that macrophage infiltration in the LV myocardium was reduced in the ATV-L and ATV-H groups compared with the MetS group (Figure 2A, B). The abundance of MCP-1 and COX-2 mRNAs in LV tissue of MetS rats was also decreased by atorvastatin (Figure 2C, D).

3.5. Cardiac AMPK and NF-κB Activation

Immunoblot analysis showed that atorvastatin up-regulated AMPK phosphorylation and down-regulated phosphorylation of the p65 subunit of NF-κB in DS/obese rat hearts (Figure 2E, F).

3.6. Adipocyte Hypertrophy and Adipose Tissue Inflammation

The high dose of atorvastatin reduced the cross-sectional area of adipocytes in visceral adipose tissue of MetS rats to a greater extent than did the low dose (Figure 3A, B). Macrophage infiltration in adipose tissue was decreased in the ATV-L and ATV-H groups (Figure 3C). The amounts of MCP-1 and COX-2 mRNAs in adipose tissue were similarly down-regulated by both doses of atorvastatin (Figure 3D, E).

3.7. Circulating Adiponectin Level and Expression of Adiponectin, PPARγ, and SREBP-1c Genes in Adipose Tissue

The concentration of adiponectin in serum in MetS rats was significantly reduced by atorvastatin at both doses (Table 1). The abundance of adiponectin mRNA in adipose tissue was decreased in MetS rats in a manner sensitive to atorvastatin (Figure 3F). Atorvastatin also attenuated the increases in the abundance of PPARγ and SREBP-1c mRNAs in DS/obese rat adipose tissues (Figure 3G, H).

3.8. Expression of PPARγ Protein and Activation of AMPK, NF-κB p65, p70S6K, and Akt in Adipose Tissue

The abundance of PPARγ protein in adipose tissue was increased in MetS rats, and this effect was abolished by treatment with atorvastatin at either dose (Figure 3I). The phosphorylation of AMPK in adipose tissue was decreased in MetS rats and as in LV tissue, was increased by atorvastatin treatment (Figure 3J). In contrast to LV tissue, however, the extent of NF-κB p65 phosphorylation in adipose tissue was reduced in MetS rats, and this effect was further enhanced by atorvastatin (Figure 3K). The phosphorylation of p70 ribosomal protein S6 kinase (p70S6K) was increased and that of Akt was decreased in adipose tissue of MetS rats, and both of these effects were attenuated by atorvastatin treatment (Figure 3L, M).

4. Discussion

We have shown that short-term administration of atorvastatin at two different doses ameliorated LV fibrosis and diastolic dysfunction, cardiac oxidative stress and inflammation, as well as enlargement of visceral adipocytes and adipose tissue inflammation in DS/obese rats. In addition, atorvastatin induced phosphorylation (activation) of AMPK and dephosphorylation (inactivation) of the p65 subunit of NF-κB in the heart and adipose tissue. Furthermore, it ameliorated glucose intolerance and insulin resistance, but, unexpectedly, it reduced circulating adiponectin levels. Both low and high doses of atorvastatin lowered circulating concentrations of LDL-cholesterol, triglyceride, and FFAs to a similar extent. The anti-inflammatory actions of atorvastatin on the heart and adipose tissue are probably attributable, at least partly, to the increase in AMPK activity and consequent decrease in NF-κB activity.

AMPK is a nutrient and energy sensor and regulates metabolic energy balance at the whole-body level. AMPK signaling also inhibits inflammatory responses induced

by activation of the NF-κB system [8]. The heterodimeric protein NF-κB is a ubiquitous redox-sensitive transcription factor that remains sequestered in the cytosol as an inactive complex with its endogenous inhibitor IκB-α under basal conditions. The p65 subunit of NF-κB contains the activation domain and determines the transactivation activity of NF-κB [28]. Oxidative or inflammatory stimuli, including tumor necrosis factor–α (TNF-α), induce phosphorylation and subsequent proteasomal degradation of IκB-α, thereby releasing the NF-κB dimer and allowing its translocation to the nucleus [29]. Indeed, both the decrease in phosphorylation of AMPK and the increase in that of the p65 subunit of NF-kB have been associated with increased oxidative stress and inflammation in the heart of DS/obese rats [27]. Atorvastatin induced the phosphorylation (activation) of AMPK as well as the dephosphorylation (inactivation) of NF-κB p65 in these hearts. Atorvastatin and other statins have previously been shown to activate AMPK by inducing its phosphorylation at Thr^{172} both in vitro and in vivo, with this effect resulting in activation of endothelial nitric oxide synthase and contributing to pleiotropic effects of statins that benefit the cardiovascular system [6]. It is reported that protein kinase C-ζ, calcium/calmodulin-dependent protein kinase kinase β, and the protein kinase LKB1 are involved in statin-induced AMPK phosphorylation [30, 31]. AMPK can inhibit NF-κB activity not directly but through its downstream mediators, sirtuin 1, p53, PPARγ co-activator 1α and Forkhead box O family [8]. In addition, AMPK inhibits endoplasmic reticulum and oxidative stresses which can induce NF-κB activation. Our results now suggest that atorvastatin attenuated cardiac inflammation by inducing activation of AMPK and consequent inactivation of NF-κB and thereby ameliorated cardiac remodeling and diastolic dysfunction.

The NF-κB pathway is thought to be activated in obese adipose tissue, in which

cross talk between adipocytes and macrophages gives rise to a proinflammatory vicious circle [32]. However, we found that activation of NF-κB p65 was attenuated in the adipose tissue of DS/obese rats compared with that of DS/lean rats, consistent with the previous observation in mice with fat-specific knockout of p65 that NF-κB is required for inhibition of adipocyte apoptosis in the obese condition, with NF-κB inactivation promoting adipose tissue inflammation through induction of adipocyte apoptosis [33]. NF-κB may therefore have an anti-inflammatory effect in adipose tissue in obesity that is mediated by inhibition of apoptosis. Our results also suggest that exceeding the critical visceral adipose tissue threshold [34] may have resulted in the down-regulation of NF-κB activity and consequent induction of apoptosis in adipocytes, leading to adipose tissue inflammation. In the obese condition, therefore, NF-κB activation may be an inflammatory marker in the heart but not in adipose tissue. Atorvastatin inhibited inflammation as well as further reduced NF-κB activity in DS/obese rat adipose tissues, consistent with previous results showing that this drug suppressed the phosphorylation of both the upstream kinases IκB kinase (IKK)-β and IKK-α in obese mouse adipose tissues [12], and that statins inhibit NF-κB activation in several cell types [35] as well as inhibit the expression of inducers of NF-κB signaling such as TNF-α [36] and interleukin-6 [37]. Our results thus suggest that inhibition of NF-κB signaling with atorvastatin may be mediated though downstream targets of AMPK.

SREBP-1c is a transcription factor that induces the expression of various genes related to glucose utilization and fatty acid synthesis [38]. The up-regulation of SREBP-1c mRNA as well as that of PPARγ expression in DS/obese rat adipose tissues are in agreement with previous results showing that SREBP-1c promotes adipocyte

differentiation and thereby mediates the production of a PPARγ-activating ligand and contributes to the development of adipocyte hypertrophy [39]. Atorvastatin was previously shown to increase the expression of PPARs (PPARα, -β, -γ, and -δ) as well as to attenuate the expression of proinflammatory cytokines in the rat heart [40]. We found that atorvastatin down-regulated PPARγ expression in adipose tissue of DS/obese rats, suggesting that the anti-inflammatory effects of atorvastatin in adipose tissue are independent of PPARγ and are instead mediated by activation of AMPK.

We have previously shown that, unlike that in human MetS, the serum adiponectin concentration is elevated in DS/obese rats [27, 41]. This elevation was attenuated by treatment with atorvastatin. In contrast, expression of the adiponectin gene was down-regulated in adipose tissue of DS/obese rats in a manner sensitive to atorvastatin treatment. Adiponectin-induced activation of AMPK in the heart is thought to underlie the cardioprotective effect of adiponectin in mice [42]. Unexpectedly, therefore, the increase in the circulating adiponectin level in DS/obese rats is accompanied by a decrease in cardiac AMPK activity, and the fall in the circulating adiponectin level induced by atorvastatin treatment was associated with an increase in cardiac AMPK activity. Although the reason for the apparent discrepancy between the circulating level of adiponectin and adiponectin gene expression in adipose tissue of DS/obese rats remains unclear, it might be related in part to changes in the expression of adiponectin binding proteins such as adiponectin receptors 1 and 2 and T-cadherin [43].

Atorvastatin ameliorated both insulin resistance and glucose intolerance in DS/obese rats, with the former effect being consistent with previous results obtained with a rat model of type 2 diabetes [11] and with obese mice [12]. Given that FFAs released from enlarged adipocytes induce insulin resistance, whereas adiponectin

released from normal adipocytes enhances insulin sensitivity, our results suggest that the reductions in the circulating FFA level and in adipocyte size induced by atorvastatin contribute to the amelioration of insulin resistance in DS/obese rats. Atorvastatin also attenuated the down-regulation of Akt activation in adipose tissue of DS/obese rats, consistent with the previous observation that it induces phosphorylation of Akt at Ser^{473}, which plays an important role in signaling downstream of the insulin receptor [10]. Insulin activates a signaling pathway including insulin receptor substrate (IRS), Akt, mammalian target of rapamycin (mTOR), and p70S6K, the latter of which in turn phosphorylates IRS and thereby limits further insulin signaling. This feedback loop is also activated by other signals that stimulate mTOR-p70S6K including nutrients and growth factors [44]. Indeed, the phosphorylation of p70S6K and Akt was increased and decreased, respectively, in adipose tissue of DS/obese rats [20]. AMPK maintains energy homeostasis and negatively regulates mTOR complex 1 (mTORC1) activity [45]. Atorvastatin alleviated the decrease in AMPK activity as well as the increase in p70S6K activity in DS/obese rat adipose tissues, suggesting that activation of AMPK by atorvastatin inhibited mTORC1-p70S6K signaling and thereby increased phosphorylation of Akt at Ser^{473} and ameliorated insulin resistance [20].

5. Conclusions

Atorvastatin reduced LV fibrosis and diastolic dysfunction, cardiac oxidative stress and inflammation, as well as adipocyte hypertrophy and inflammation in visceral adipose tissue in DS/obese rats. It also alleviated insulin resistance and glucose intolerance despite a decrease in circulating adiponectin levels. The present results suggest that the anti-inflammatory effects of atorvastatin on the heart and adipose tissue are related, at least in part, to increased AMPK activity and decreased NF-κB activity. Further studies

are needed to elucidate the molecular mechanisms responsible for these actions of atorvastatin.

Acknowledgments

We thank Yuji Minagawa, Takuya Hattori, and Shogo Watanabe for technical assistance.

References

[1] Heart Protection Study Collaborative Group, MRC/BHF Heart Protection Study of cholesterol lowering with simvastatin in 20,536 high-risk individuals: a randomised placebo-controlled trial, Lancet. 360 (2002) 7-22.

[2] J. Shepherd, S.M. Cobbe, I. Ford, et al., Prevention of coronary heart disease with pravastatin in men with hypercholesterolemia. West of Scotland Coronary Prevention Study Group, N. Engl. J. Med. 333 (1995) 1301-1307.

[3] S. Ichihara, A. Noda, K. Nagata, et al., Pravastatin increases survival and suppresses an increase in myocardial matrix metalloproteinase activity in a rat model of heart failure, Cardiovasc. Res. 69 (2006) 726-735.

[4] M. Saka, K. Obata, S. Ichihara, et al., Pitavastatin improves cardiac function and survival in association with suppression of the myocardial endothelin system in a rat model of hypertensive heart failure, J. Card. Pharm. 47 (2006) 770-779.

[5] J.S. Forrester, P. Libby, The inflammation hypothesis and its potential relevance to statin therapy, Am. J. Cardiol. 99 (2007) 732-738.

[6] W. Sun, T.S. Lee, M. Zhu, et al., Statins activate AMP-activated protein kinase in vitro and in vivo, Circulation. 114 (2006) 2655-2662.

[7] Y. Kureishi, Z. Luo, I. Shiojima, et al., The HMG-CoA reductase inhibitor simvastatin activates the protein kinase Akt and promotes angiogenesis in normocholesterolemic animals, Nat. Med. 6 (2000) 1004-1010.

[8] A. Salminen, J.M. Hyttinen, K. Kaarniranta, AMP-activated protein kinase inhibits NF-kappaB signaling and inflammation: impact on healthspan and lifespan, J. Mol. Med. (Berl.). 89 (2011) 667-676.

[9] M. Brault, J. Ray, Y.H. Gomez, C.S. Mantzoros, S.S. Daskalopoulou, Statin treatment and new-onset diabetes: a review of proposed mechanisms, Metabolism. 63 (2014) 735-745.

[10] V. Wong, L. Stavar, L. Szeto, et al., Atorvastatin induces insulin sensitization in Zucker lean and fatty rats, Atherosclerosis. 184 (2006) 348-355.

[11] Y. Chen, K. Ohmori, M. Mizukawa, et al., Differential impact of atorvastatin vs pravastatin on progressive insulin resistance and left ventricular diastolic dysfunction in a rat model of type II diabetes, Circ. J. 71 (2007) 144-152.

[12] D.T. Furuya, A.C. Poletto, R.R. Favaro, J.O. Martins, T.M. Zorn, U.F. Machado, Anti-inflammatory effect of atorvastatin ameliorates insulin resistance in monosodium glutamate-treated obese mice, Metabolism. 59 (2010) 395-399.

[13] T. Hattori, T. Murase, M. Ohtake, et al., Characterization of a new animal model of metabolic syndrome: the DahlS.Z-*Lepr*^{fa}/*Lepr*^{fa} rat, Nutr. Diabetes. 1 (2011) e1.

[14] T. Murase, T. Hattori, M. Ohtake, et al., Cardiac remodeling and diastolic dysfunction in DahlS.Z-*Lepr*^{fa}/*Lepr*^{fa} rats: a new animal model of metabolic syndrome, Hypertens. Res. 35 (2012) 186-193.

[15] N. Matsuura, K. Nagasawa, Y. Minagawa, et al., Restraint stress exacerbates cardiac and adipose tissue pathology via beta-adrenergic signaling in rats with metabolic syndrome, Am. J. Physiol. Heart Circ. Physiol. 308 (2015) H1275-1286.

[16] K. Nagasawa, N. Matsuura, Y. Takeshita, et al., Attenuation of cold stress-induced exacerbation of cardiac and adipose tissue pathology and metabolic disorders in a rat model of metabolic syndrome by the glucocorticoid receptor antagonist RU486, Nutr. Diabetes. 6 (2016) e207.

[17] Y. Takeshita, S. Watanabe, T. Hattori, et al., Blockade of glucocorticoid receptors with RU486 attenuates cardiac damage and adipose tissue inflammation in a rat model of metabolic syndrome, Hypertens. Res. 38 (2015) 741-750.

[18] K. Nagata, F. Somura, K. Obata, et al., AT1 receptor blockade reduces cardiac calcineurin activity in hypertensive rats, Hypertension. 40 (2002) 168-174.

[19] Y. Yamada, K. Tsuboi, T. Hattori, et al., Mechanism underlying the efficacy of combination therapy with losartan and hydrochlorothiazide in rats with salt-sensitive hypertension, Hypertens. Res. 34 (2011) 809-816.

[20] T. Hattori, T. Murase, M. Takatsu, et al., Dietary salt restriction improves cardiac and adipose tissue pathology independently of obesity in a rat model of metabolic syndrome, J. Am. Heart Assoc. 3 (2014) e001312.

[21] C.H. Sales, A.R. Santos, D.E. Cintra, C. Colli, Magnesium-deficient high-fat diet: effects on adiposity, lipid profile and insulin sensitivity in growing rats, Clin. Nutr. 33 (2014) 879-888.

[22] A.A. Elmarakby, E.D. Loomis, J.S. Pollock, D.M. Pollock, NADPH oxidase inhibition attenuates oxidative stress but not hypertension produced by chronic ET-1, Hypertension. 45 (2005) 283-287.

[23] K. Takahashi, M. Takatsu, T. Hattori, et al., Premature cardiac senescence in DahlS.Z-*Lepr*^{fa}/*Lepr*^{fa} rats as a new animal model of metabolic syndrome, Nagoya J. Med. Sci. 76 (2014) 35-49.

[24] M. Takatsu, C. Nakashima, K. Takahashi, et al., Calorie restriction attenuates cardiac remodeling and diastolic dysfunction in a rat model of metabolic syndrome, Hypertension. 62 (2013) 957-965.

[25] K. Nagata, K. Obata, J. Xu, et al., Mineralocorticoid receptor antagonism attenuates cardiac hypertrophy and failure in low-aldosterone hypertensive rats,

Hypertension. 47 (2006) 656-664.

[26] T. Murase, T. Hattori, M. Ohtake, et al., Effects of estrogen on cardiovascular injury in ovariectomized female DahlS.Z-*Lepr*^{fa}/*Lepr*^{fa} rats as a new animal model of metabolic syndrome, Hypertension. 59 (2012) 694-704.

[27] S. Ito, Y. Sano, K. Nagasawa, et al., Highly purified eicosapentaenoic acid ameliorates cardiac injury and adipose tissue inflammation in a rat model of metabolic syndrome, Obes. Sci. Pract. 2 (2016) 318-329.

[28] R.G. Baker, M.S. Hayden, S. Ghosh, NF-kappaB, inflammation, and metabolic disease, Cell Metab. 13 (2011) 11-22.

[29] Y.J. Surh, J.K. Kundu, H.K. Na, J.S. Lee, Redox-sensitive transcription factors as prime targets for chemoprevention with anti-inflammatory and antioxidative phytochemicals, J. Nutr. 135 (2005) 2993s-3001s.

[30] H.C. Choi, P. Song, Z. Xie, et al., Reactive nitrogen species is required for the activation of the AMP-activated protein kinase by statin in vivo, J. Biol. Chem. 283 (2008) 20186-20197.

[31] R. Kou, J. Sartoretto, T. Michel, Regulation of Rac1 by simvastatin in endothelial cells: differential roles of AMP-activated protein kinase and calmodulin-dependent kinase kinase-beta, J. Biol. Chem. 284 (2009) 14734-14743.

[32] T. Suganami, K. Tanimoto-Koyama, J. Nishida, et al., Role of the Toll-like receptor 4/NF-kappaB pathway in saturated fatty acid-induced inflammatory changes in the interaction between adipocytes and macrophages, Arterioscler. Thromb. Vasc. Biol. 27 (2007) 84-91.

[33] Z. Gao, J. Zhang, T.M. Henagan, et al., P65 inactivation in adipocytes and macrophages attenuates adipose inflammatory response in lean but not in obese mice, Am. J. Physiol. Endocrinol. Metab. 308 (2015) E496-505.

[34] E.S. Freedland, Role of a critical visceral adipose tissue threshold (CVATT) in metabolic syndrome: implications for controlling dietary carbohydrates: a review, Nutr. Metab. (Lond.). 1 (2004) 12.

[35] A. Planavila, J.C. Laguna, M. Vazquez-Carrera, Atorvastatin improves peroxisome proliferator-activated receptor signaling in cardiac hypertrophy by preventing nuclear factor-kappa B activation, Biochim. Biophys. Acta. 1687 (2005) 76-83.

[36] S. Youssef, O. Stuve, J.C. Patarroyo, et al., The HMG-CoA reductase inhibitor, atorvastatin, promotes a Th2 bias and reverses paralysis in central nervous system autoimmune disease, Nature. 420 (2002) 78-84.

[37] V. van Harmelen, T. Skurk, K. Rohrig, H. Hauner, HMG-CoA reductase inhibitor

cerivastatin inhibits interleukin-6 expression and secretion in human adipocytes, Horm. Metab. Res. 35 (2003) 466-470.

[38] P. Ferre, F. Foufelle, SREBP-1c transcription factor and lipid homeostasis: clinical perspective, Horm. Res. 68 (2007) 72-82.

[39] J.B. Kim, B.M. Spiegelman, ADD1/SREBP1 promotes adipocyte differentiation and gene expression linked to fatty acid metabolism, Genes Dev. 10 (1996) 1096-1107.

[40] L. Han, M. Li, Y. Liu, C. Han, P. Ye, Atorvastatin may delay cardiac aging by upregulating peroxisome proliferator-activated receptors in rats, Pharmacology. 89 (2012) 74-82.

[41] N. Matsuura, C. Asano, K. Nagasawa, et al., Effects of pioglitazone on cardiac and adipose tissue pathology in rats with metabolic syndrome, Int. J. Cardiol. 179 (2015) 360-369.

[42] J.R. Dyck, The ischemic heart: starving to stimulate the adiponectin-AMPK signaling axis, Circulation. 116 (2007) 2779-2781.

[43] K. Matsuda, Y. Fujishima, N. Maeda, et al., Positive feedback regulation between adiponectin and T-cadherin impacts adiponectin levels in tissue and plasma of male mice, Endocrinology. 156 (2015) 934-946.

[44] T. Haruta, T. Uno, J. Kawahara, et al., A rapamycin-sensitive pathway down-regulates insulin signaling via phosphorylation and proteasomal degradation of insulin receptor substrate-1, Mol. Endocrinol. 14 (2000) 783-794.

[45] K. Inoki, T. Zhu, K.L. Guan, TSC2 mediates cellular energy response to control cell growth and survival, Cell. 115 (2003) 577-590.

Figure Legends

Figure 1. Changes in body weight (**A**), food intake (**B**), and SBP (**C**) with age as well as time courses for an OGTT (**D**) and ITT (**E**) performed at 13 weeks of age for rats in the four experimental groups. Data are means ± SEM (n = 11, 13, 13, and 13 animals for CONT, MetS, ATV-L, and ATV-H groups, respectively). *P < 0.05 vs. CONT; †P < 0.05 vs. MetS.

Figure 2. Macrophage infiltration, inflammatory gene expression, as well as AMPK and NF-κB activation status in the left ventricle of rats in the three experimental groups at 13 weeks of age. (**A**) Immunohistochemical analysis with antibodies to CD68. Scale bars, 50 μm. (**B**) Density of CD68-positive cells determined from sections similar to those in (A). (**C**, **D**) Quantitative RT-PCR analysis of MCP-1 and COX-2 mRNAs, respectively. The amount of each mRNA was normalized by that of 18S rRNA and then expressed relative to the mean value for the MetS group. (**E**, **F**) Immunoblot analysis of total and phosphorylated (activated) forms of AMPK and the p65 subunit of NF-κB, respectively. Representative immunoblots as well as the ratio of phosphorylated (p-) to total forms of AMPK and p65 expressed relative to the mean value for the MetS group are shown. All quantitative data are means ± SEM [n = 13 (B) or n = 6 (C–F) animals for each group]. *P < 0.05 vs. MetS.

Figure 3. Adipocyte size, macrophage infiltration, inflammatory and adipocyte-related gene expression, and signaling protein activity in visceral (retroperitoneal) adipose tissue of rats in the three (A–E) or four (F–M) experimental groups at 13 weeks of age. (**A**) Immunohistochemical analysis with antibodies to CD68. Scale bars, 100 μm. (**B**)

Cross-sectional area of adipocytes determined from sections similar to those in (A). (**C**) Number of nuclei of CD68-positive cells as a percentage of total nuclei determined from sections similar to those in (A). (**D–H**) Quantitative RT-PCR analysis of MCP-1, COX-2, adiponectin, PPARγ, and SREBP-1c mRNAs, respectively. The amount of each mRNA was normalized by that of 18S rRNA and then expressed relative to the mean value for the MetS (D, E) or CONT (F–H) group. (**I–M**) Immunoblot analysis of PPARγ abundance as well as of AMPK, NF-κB p65, p70S6K, and Akt phosphorylation, respectively. Representative immunoblots as well as the ratio of the amount of PPARγ to that of GAPDH (internal control) and the ratio of phosphorylated (p-) to total forms of AMPK, NF-κB p65, p70S6K, and Akt expressed relative to the mean value for the CONT group are shown. All quantitative data are means ± SEM [$n = 13$ (B, C) or $n = 6$ (D–M) animals for each group]. *$P < 0.05$ vs. CONT; †$P < 0.05$ vs. MetS.

Table 1. Metabolic parameters for rats in the three experimental groups at 13 weeks of age

Parameter	MetS	ATV-L	ATV-H
Total cholesterol (mg/dL)	333.00 ± 15.6	218.00 ± 26.0*	200.33 ± 44.7*
LDL-cholesterol (mg/dL)	102.50 ± 9.37	66.00 ± 9.10*	57.25 ± 13.15*
HDL-cholesterol (mg/dL)	97.25 ± 15.33	94.83 ± 6.35	99.71 ± 5.83
Triglyceride (mg/dL)	2196.13 ± 204.52	1190.00 ± 324.22*	980.67 ± 302.75*
FFAs (mEq/L)	1.42 ± 0.14	0.61 ± 0.05*	0.59 ± 0.03*
Fasting serum glucose (mg/dL)	149.40 ± 12.36	143.00 ± 14.78	154.33 ± 15.15
Fasting serum insulin (ng/mL)	8.07 ± 0.73	4.29 ± 1.38*	4.34 ± 1.52*
HOMA-IR	83.51 ± 21.43	31.21 ± 9.52*	31.67 ± 8.05*
HOMA-β	1007.35 ± 96.24	541.02 ± 123.76*	373.35 ± 171.92*
Serum adiponectin (μg/mL)	5.19 ± 0.18	4.49 ± 0.13*	4.22 ± 0.21*

Data are means ± SEM (n = 6, 7, and 7 animals for MetS, ATV-L, and ATV-H groups, respectively). LDL, low-density lipoprotein; HDL, high-density lipoprotein; FFAs, free fatty acids; HOMA-IR, homeostasis model assessment of insulin resistance; HOMA-β, homeostasis model assessment of β-cell function. *$P < 0.05$ vs. MetS.

Figure 1

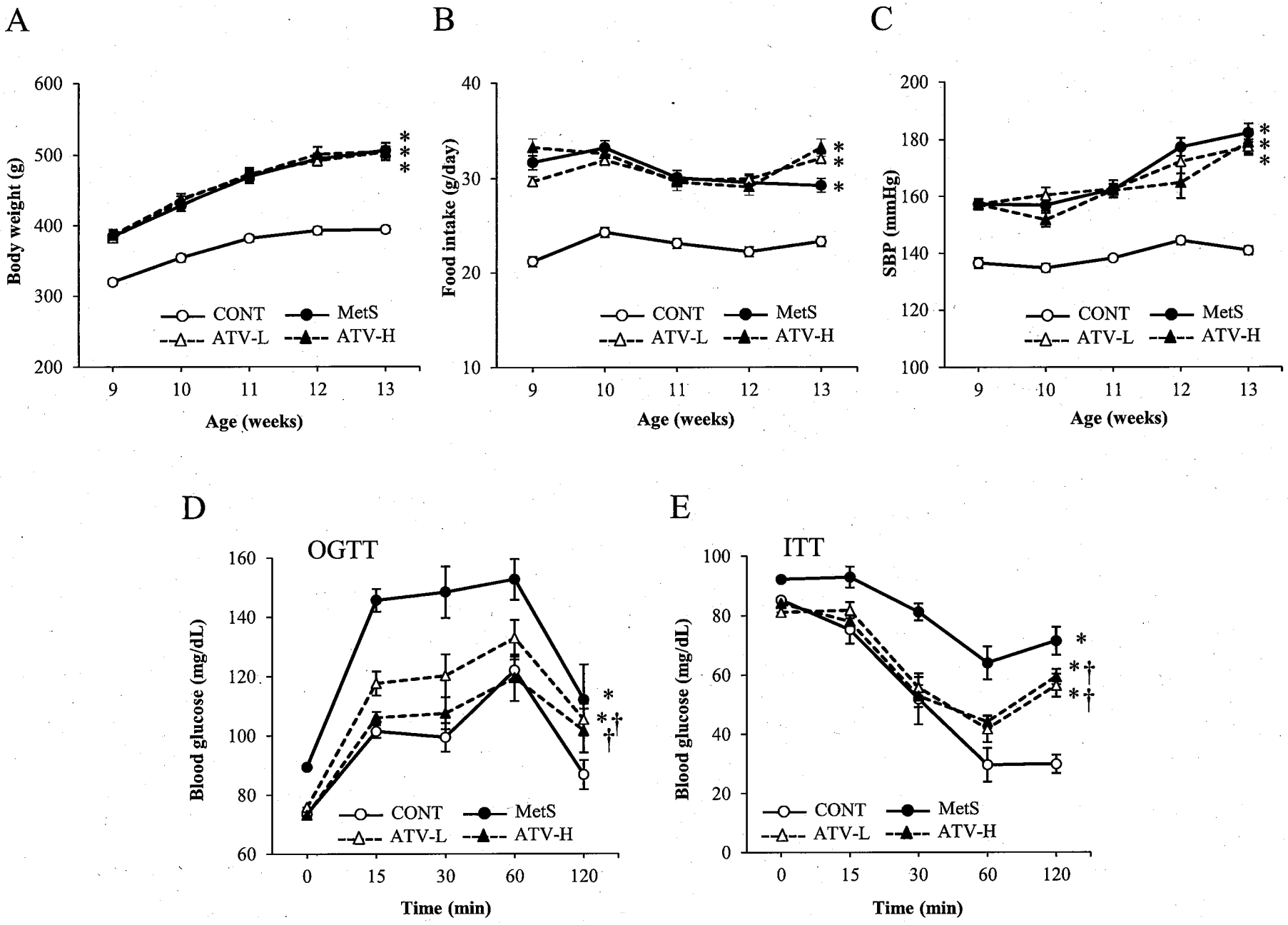
A
Body weight (g)
600
500
400
300
200
9
10
11
12
13
Age (weeks)
CONT
MetS
ATV-L
ATV-H
B
Food intake (g/day)
40
30
20
10
C
SBP (mmHg)
200
180
160
140
120
100
D
OGTT
Blood glucose (mg/dL)
160
140
120
100
80
60
0
15
30
60
120
Time (min)
E
ITT

Figure 2

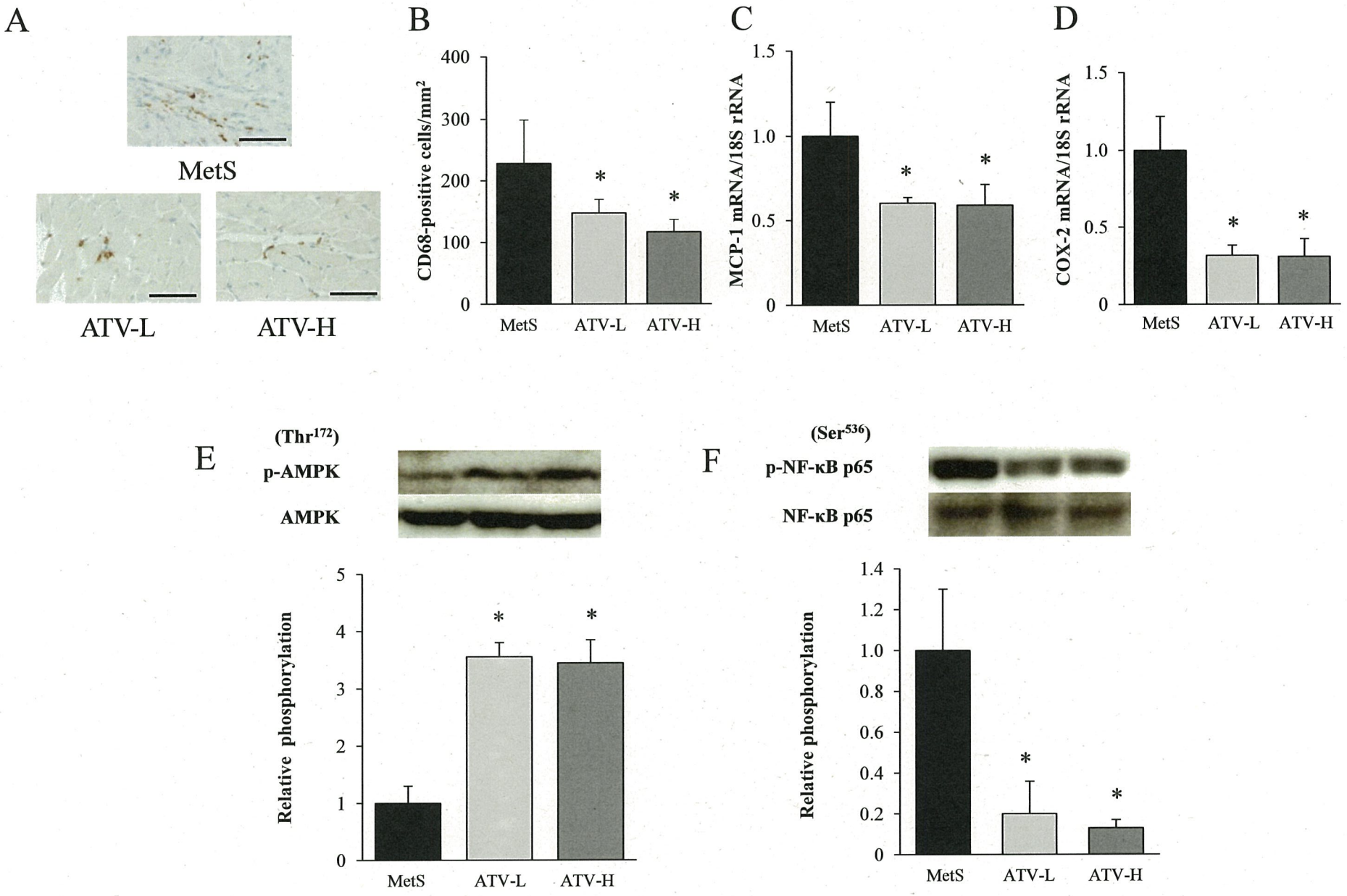
A
MetS
ATV-L
ATV-H
B
CD68-positive cells/mm²
400
300
200
100
0
MetS
ATV-L
ATV-H
C
MCP-1 mRNA/18S rRNA
1.5
1.0
0.5
0
D
COX-2 mRNA/18S rRNA
E
(Thr172)
p-AMPK
AMPK
Relative phosphorylation
5
4
3
2
1
F
(Ser536)
p-NF-κB p65
NF-κB p65
1.4
1.2
0.8
0.6
0.4
0.2

Figure 3

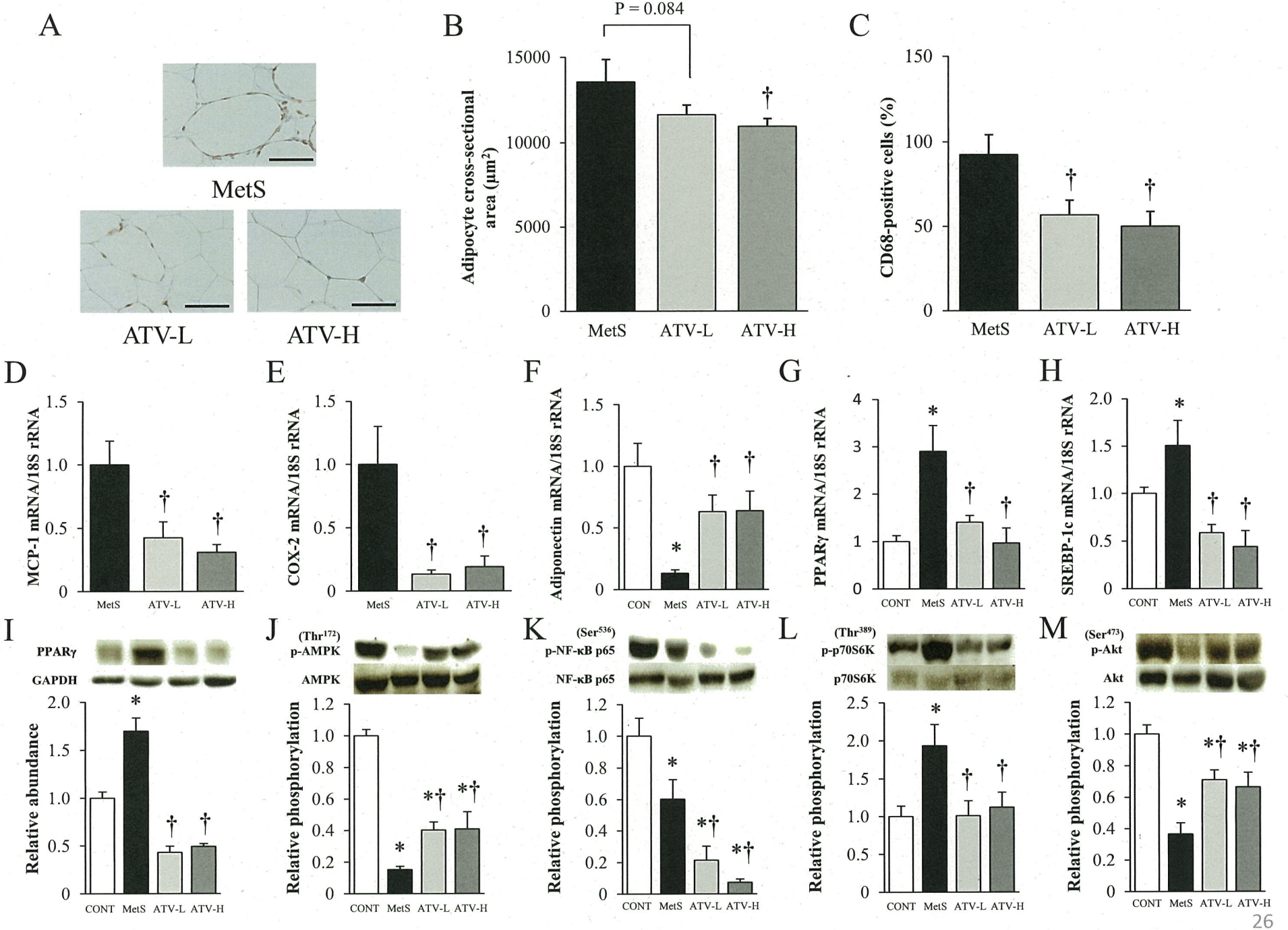
A
MetS
ATV-L
ATV-H
B
P = 0.084
Adipocyte cross-sectional area (μm²)
15000
10000
5000
0
MetS
ATV-L
ATV-H
C
CD68-positive cells (%)
150
100
50
0
MetS
ATV-L
ATV-H
D
MCP-1 mRNA/18S rRNA
E
COX-2 mRNA/18S rRNA
F
Adiponectin mRNA/18S rRNA
CON
MetS
ATV-L
ATV-H
G
PPARγ mRNA/18S rRNA
CONT
MetS
ATV-L
ATV-H
H
SREBP-1c mRNA/18S rRNA
I
PPARγ
GAPDH
Relative abundance
J
(Thr172) p-AMPK
AMPK
Relative phosphorylation
K
(Ser536) p-NF-κB p65
NF-κB p65
Relative phosphorylation
L
(Thr389) p-p70S6K
p70S6K
Relative phosphorylation
M
(Ser473) p-Akt
Akt
Relative phosphorylation

Supplemental Methods

Animals

Animal experiments were approved by the Animal Experiment Committee of Nagoya University Graduate School of Medicine (Daiko distinct, approval nos. 025-035, 026-010, 027-003, and 028-012). Eight-week-old male inbred DahlS.Z-*Lepr*^{fa}/*Lepr*^{fa} rats were obtained from Japan SLC Inc. (Hamamatsu, Japan). Animals were handled in accordance with the Regulations for Animal Experiments at Nagoya University as well as with the Guide for the Care and Use of Laboratory Animals (U.S. National Institutes of Health publication No. 85-23, revised 2011). The feeding protocol was described in our previous publication [1]. The doses of atorvastatin were determined from previous results [2-4]. Body weight and food intake were monitored weekly.

Supplemental References

[1] K. Nagasawa, N. Matsuura, Y. Takeshita, et al., Attenuation of cold stress-induced exacerbation of cardiac and adipose tissue pathology and metabolic disorders in a rat model of metabolic syndrome by the glucocorticoid receptor antagonist RU486, Nutr. Diabetes. 6 (2016) e207.

[2] V. Wong, L. Stavar, L. Szeto, et al., Atorvastatin induces insulin sensitization in Zucker lean and fatty rats, Atherosclerosis. 184 (2006) 348-355.

[3] D.T. Furuya, A.C. Poletto, R.R. Favaro, J.O. Martins, T.M. Zorn, U.F. Machado, Anti-inflammatory effect of atorvastatin ameliorates insulin resistance in monosodium glutamate-treated obese mice, Metabolism. 59 (2010) 395-399.

[4] Y. Chen, K. Ohmori, M. Mizukawa, et al., Differential impact of atorvastatin vs pravastatin on progressive insulin resistance and left ventricular diastolic dysfunction in a rat model of type II diabetes, Circ. J. 71 (2007) 144-152.

Supplemental Figure Legends

Figure S1. Cardiomyocyte size, fibrosis, and expression of fetal-type cardiac and fibrosis-related genes in the left ventricle of rats in the three experimental groups at 13 weeks of age. (**A**) Hematoxylin-eosin staining of transverse sections of the LV myocardium. Scale bars, 50 μm. (**B**) Cross-sectional area of cardiac myocytes determined from sections similar to those in (A). (**C**, **D**) Quantitative reverse transcription (RT) and polymerase chain reaction (PCR) analysis of ANP and BNP mRNAs, respectively. The amount of each mRNA was normalized by that of 18S rRNA and then expressed relative to the mean value for the MetS group. (**E**, **F**) Collagen deposition as revealed by Azan-Mallory staining in perivascular and interstitial regions of the LV myocardium, respectively. Scale bars, 200 and 100 μm, respectively. (**G**, **H**) Relative extents of perivascular and interstitial fibrosis, respectively, as determined from sections similar to those in (E) and (F). (**I–L**) Quantitative RT-PCR analysis of collagen types I and III, CTGF, and TGF-β1 mRNAs, respectively. All quantitative data are means ± SEM [$n = 13$ (B, G, H) or $n = 6$ (C, D, I–L) animals for each group]. $^*P < 0.05$ vs. MetS.

Figure S2. NADPH oxidase activity and gene expression in the left ventricle of rats in the three experimental groups at 13 weeks of age. (**A**) Superoxide production as revealed by dihydroethidium staining in interstitial regions of the LV myocardium. Scale bars, 100 μm. (**B**) Relative dihydroethidium fluorescence intensity determined from sections similar to those in (A). (**C**) NADPH-dependent superoxide production in LV homogenates. Results are expressed as relative light units (RLU) per minute per milligram of protein. (**D–F**) Quantitative RT-PCR analysis of $p22^{phox}$, $gp91^{phox}$, and

Rac1 mRNAs, respectively. The amount of each mRNA was normalized by that of 18S rRNA and then expressed relative to the mean value for the MetS group. All quantitative data are means ± SEM [$n = 13$ (B, C) or $n = 6$ (D–F) animals for each group]. *$P < 0.05$ vs. MetS.

Supplemental Tables

Table S1. Sequences of oligonucleotide primers for quantitative RT-PCR analysis of rat mRNAs.

Target	Sequence	GenBank accession no.
Adiponectin		NM_144744
Forward	5'-GCCCTACGCTGAATGCTGAG-3'	
Reverse	5'-GAACCCCTGGCAGGAAAGG-3'	
PPARγ		NM_013124
Forward	5'-GGAGTCCATGCTTGTGAAGG-3'	
Reverse	5'-GCAAGGACTTTATGTATGAG-3'	
SREBP-1c		AF286470
Forward	5'-CGCTACCGTTCCTCTATCAATGAC-3'	
Reverse	5'-AGTTTCTGGTTGCTGTGCTGTAAG-3'	

Abbreviations: RT-PCR, reverse transcription and polymerase chain reaction; PPARγ, peroxisome proliferator-activated receptor γ; SREBP-1c, sterol regulatory element-binding protein-1c

Table S2. Weights of various tissues relative to tibial length (TL) for rats in the three experimental groups at 13 weeks of age

Parameter	MetS	ATV-L	ATV-H
TL (mm)	34.62 ± 0.15	34.58 ± 0.15	34.52 ± 0.21
Heart/TL (mg/mm)	42.95 ± 1.15	42.18 ± 0.99	42.78 ± 1.06
Left ventricle/TL (mg/mm)	31.01 ± 0.90	29.93 ± 0.82	30.82 ± 0.89
Retroperitoneal fat/TL (mg/mm)	429.56 ± 13.64	415.13 ± 12.15	429.58 ± 14.03
Epididymal fat/TL (mg/mm)	354.81 ± 9.75	358.00 ± 11.72	362.10 ± 9.36
Mesenteric fat/TL (mg/mm)	364.22 ± 10.33	371.46 ± 9.60	348.17 ± 9.57
Inguinal fat/TL (mg/mm)	1501.32 ± 68.53	1448.07 ± 60.58	1482.16 ± 53.88

Data are means ± SEM (n = 13 animals for each group).

Table S3. Cardiac morphology and function for rats in the four experimental groups at 13 weeks of age

Parameter	MetS	ATV-L	ATV-H
IVSTd (mm)	2.06 ± 0.03	1.96 ± 0.02	1.99 ± 0.04
LVDd (mm)	8.27 ± 0.13	8.56 ± 0.08	8.43 ± 0.11
LVPWTd (mm)	2.06 ± 0.06	1.96 ± 0.04	1.99 ± 0.06
LV mass (mg)	1292 ± 38	1212 ± 18	1237 ± 37
RWT	0.49 ± 0.01	0.46 ± 0.01	0.47 ± 0.02
LVFS (%)	47.66 ± 2.43	43.53 ± 1.18	44.28 ± 1.60
LVEF (%)	82.50 ± 1.94	79.33 ± 1.21	79.88 ± 1.51
DcT (ms)	53.05 ± 1.48	46.93 ± 1.06*	43.5 ± 1.57*
IRT (ms)	40.75 ± 2.42	32.78 ± 1.14*	29.2 ± 1.79*
Tau (ms)	33.52 ± 1.09	25.89 ± 1.53*	22.53 ± 0.89*
LVEDP (mmHg)	17.65 ± 1.43	10.39 ± 2.03*	8.77 ± 1.87*
LVEDP/LVDd (mmHg/mm)	2.10 ± 0.13	1.20 ± 0.25*	1.05 ± 0.24*

Data are means ± SEM (n = 13 animals for each group). IVSTd, interventricular septum thickness in diastole; LVDd, left ventricular end-diastolic dimension; LVPWTd, LV posterior wall thickness in diastole; RWT, relative wall thickness; LVFS, LV fractional shortening; LVEF, LV ejection fraction; DcT, deceleration time; IRT, isovolumic relaxation time; LVEDP, LV end-diastolic pressure. *P < 0.05 vs. MetS.

Figure S1

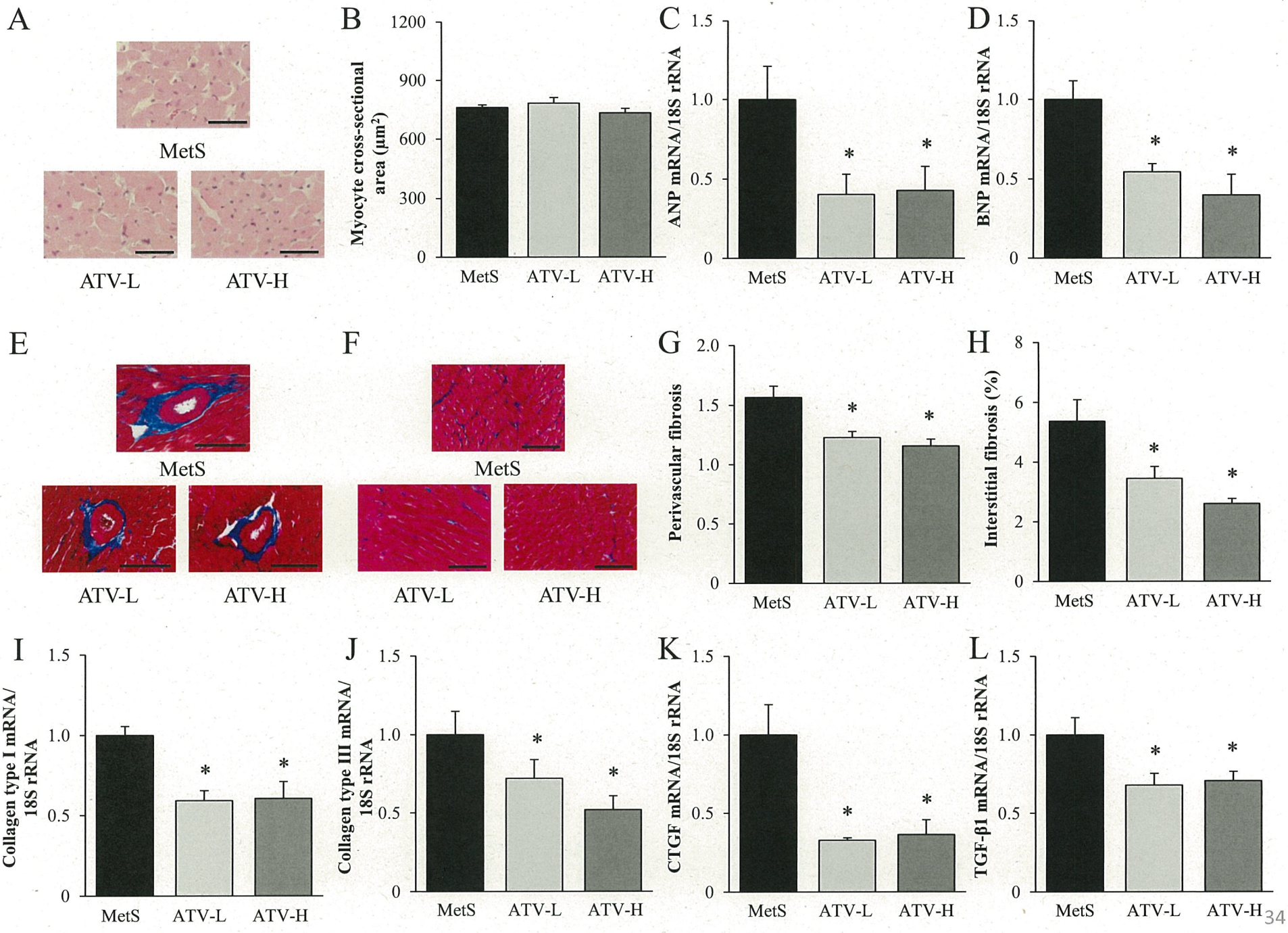
A
MetS
ATV-L
ATV-H
B
Myocyte cross-sectional area (μm²)
1200
900
600
300
0
MetS
ATV-L
ATV-H
C
ANP mRNA/18S rRNA
1.5
1.0
0.5
0
*
D
BNP mRNA/18S rRNA
E
F
G
Perivascular fibrosis
2.0
1.5
1.0
0.5
H
Interstitial fibrosis (%)
8
6
4
2
I
Collagen type I mRNA/ 18S rRNA
J
Collagen type III mRNA/ 18S rRNA
K
CTGF mRNA/18S rRNA
L
TGF-β1 mRNA/18S rRNA

Figure S2

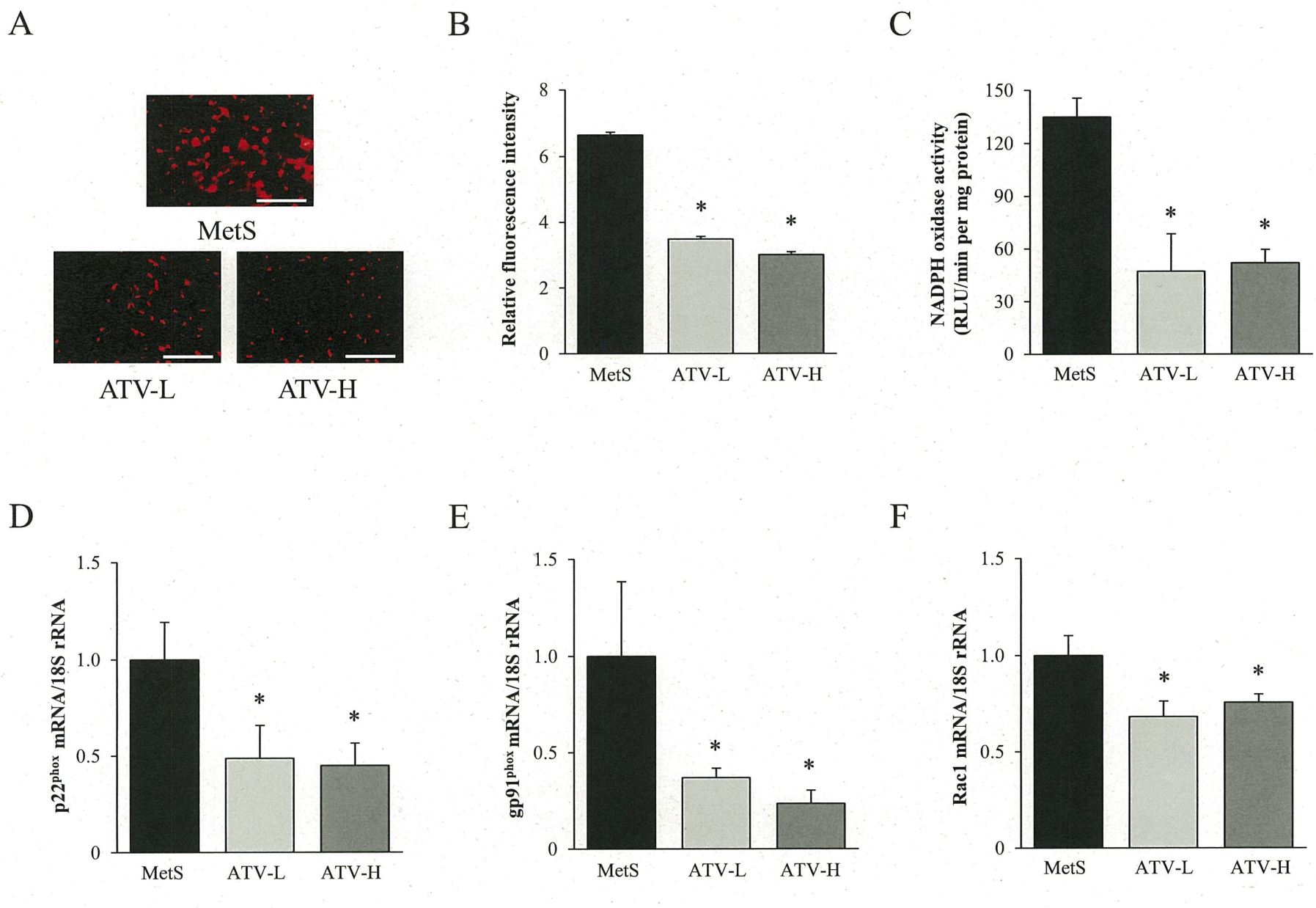
A
MetS
ATV-L
ATV-H
B
Relative fluorescence intensity
0
2
4
6
8
MetS
ATV-L
ATV-H
C
NADPH oxidase activity
(RLU/min per mg protein)
0
30
60
90
120
150
MetS
ATV-L
ATV-H
D
p22phox mRNA/18S rRNA
0
0.5
1.0
1.5
MetS
ATV-L
ATV-H
E
gp91phox mRNA/18S rRNA
0
0.5
1.0
1.5
MetS
ATV-L
ATV-H
F
Rac1 mRNA/18S rRNA
0
0.5
1.0
1.5
MetS
ATV-L
ATV-H